The molecular basis of the coloration mechanism in lobster shell: β-Crustacyanin at 3.2-Å resolution

Michele Cianci*, Pierre J. Rizkallah†, Andrzej Olczak*‡, James Raftery*, Naomi E. Chayen§, Peter F. Zagalsky¶, and John R. Helliwell*‖

*Department of Chemistry, University of Manchester, Manchester M13 9PL, United Kingdom; †Council for the Central Laboratory of the Research Councils Daresbury Laboratory, Daresbury, Warrington, Cheshire WA4 4AD, United Kingdom; §Biological Structure and Function Section, Division of Biomedical Sciences, Faculty of Medicine, Imperial College, London SW7 2AZ, United Kingdom; and ¶Department of Molecular Biology and Biochemistry, Royal Holloway College, University of London, Egham, Surrey TW20 OEX, United Kingdom

Edited by Gregory A. Petsko, Brandeis University, Waltham, MA, and approved May 8, 2002 (received for review February 12, 2002)

The binding of the carotenoid astaxanthin (AXT) in the protein multimacromolecular complex crustacyanin (CR) is responsible for the blue coloration of lobster shell. The structural basis of the bathochromic shift mechanism has long been elusive. A change in color occurs from the orange red of the unbound dilute AXT (λ_{max} 472 nm in hexane), the well-known color of cooked lobster, to slate blue in the protein-bound live lobster state (λ_{max} 632 nm in CR). Intriguingly, extracted CR becomes red on dehydration and on rehydration goes back to blue. Recently, the innovative use of softer x-rays and xenon derivatization yielded the three-dimensional structure of the A_1 apoprotein subunit of CR, confirming it as a member of the lipocalin superfamily. That work provided the molecular replacement search model for a crystal form of the β-CR holo complex, that is an A_1 with A_3 subunit assembly including two bound AXT molecules. We have thereby determined the structure of the A_3 molecule *de novo*. Lobster has clearly evolved an intricate structural mechanism for the coloration of its shell using AXT and a bathochromic shift. Blue/purple AXT proteins are ubiquitous among invertebrate marine animals, particularly the Crustacea. The three-dimensional structure of β-CR has identified the protein contacts and structural alterations needed for the AXT color regulation mechanism.

The bathochromic shift of the absorption by astaxanthin (AXT) (3,3′-dihydroxy-β,β′-carotene-4,4′-dione; Fig. 1) in lobster crustacyanin (CR) has intrigued scientists for over 50 years (1–4). The visible absorption spectra of free dilute AXT, of β- and α-CR peak at 472 nm in hexane or 492 nm in pyridine, 580 and 632 nm, respectively (2). Detailed chemical studies involving reconstitution with natural and chemically synthesized carotenoids (4) have established the essential chemical characteristics required for this bathochromic shift effect, which arises from a reduced energy gap between ground and excited states. Keto groups are needed at positions 4 and 4′, conjugated with the polyene chain; methyl groups are needed at the central positions C20 and C20′; only E (all trans) isomers are bound to the protein; and no great variation in overall shape and size of the carotenoid is tolerated. The visible CD spectrum of β-CR, attributed to helical twisting of the chromophore, shows exciton splitting indicating that the two AXTs are proximal (2, 4). The lowered $\nu_{C=C}$ of AXT in the resonance Raman spectra of the CRs, indicative of increased electron delocalization in the electronic ground state, has been attributed to polarization of the π-electron system by proximal charge groups or hydrogen bonds (3). These spectra argue against a large protein-induced distortion of the polyene chain, although minor changes to its geometry would be required to explain the spectra (3, 4). ^{13}C magic angle spinning NMR, together with Stark spectroscopy, gives support to an essentially symmetrical polarization of the AXT in CR with some asymmetry superimposed on the two halves of the chromophore (5, 6). A protonation model involving the C-4 keto groups at the ends of the AXT molecule, consistent with observed visible and NMR spectra, in which a water molecule is involved in the polarization process (4), has been proposed.

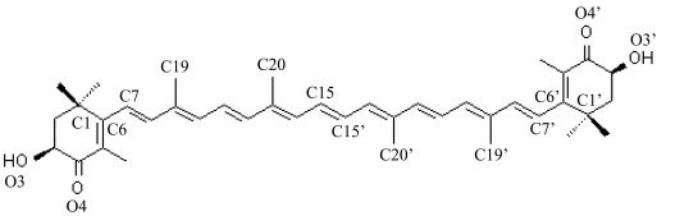

Fig. 1. The chemical scheme of the carotenoid AXT. The molecule is centrosymmetric.

There is also a putative model for the β-CR, based on the subunit amino acid sequences (7), which has an end ring of each AXT in a nonpolar proton-deficient environment of each putative lipocalin subunit. This model is inconsistent with a polarization introduced by protonation of the 4 and 4′ keto groups and with the above studies. Past analytical work has shown that this pigment–protein complex contains 16 AXT molecules and consists of an aggregation of eight 40-kDa dimeric units (β-CRs), each of which binds two molecules of AXT. The β-CRs are irreversible dissociation products of α-CRs and are combinations of two types of ≈20-kDa protomers (apoproteins) of Type I (CRTC) and Type II (CRTA) with bound carotenoids. The detailed nomenclature of the apoproteins is based on their electrophoretic mobilities and chemical properties (8): CRTC comprises apoCRs C_1, C_2, and A_1, whereas CRTA comprises A_2 and A_3. The β-dimer structure presented here is an assembly of the A_1 and A_3 proteins with two bound AXT molecules. The original interest in CR arose from the similarity of the spectral shift of AXT in CR to that of retinal in the rod visual pigment rhodopsin (1). In the retinal-binding protein family, comprising the seven-helix transmembrane proteins, the rhodopsins, and the bacteriorhodopsins, the mechanism of the spectral shifts is primarily polarization. The retinal ligand is covalently bound by a protonated Schiff base linkage, and the magnitude of the spectral shift is principally regulated by charged side-chain counterions (9, 10). In contrast, in CR the carotenoids are attached noncovalently. The reduction in the gap between ground and excited states for AXT in the complex is significant at 0.73 of that for rhodopsin. It is the same percentage-wise in both complexes (≈26%) relative to the gap. Other lipocalins bind their ligand within the calyx of a single monomer, e.g., plasma retinol-binding protein (11). Bilin-binding protein (12)

This paper was submitted directly (Track II) to the PNAS office.

Abbreviations: AXT, astaxanthin; CR, crustacyanin; CRTA/C, CR gene product A or C.

Data deposition: The atomic coordinates and structure factors have been deposited in the Protein Data Bank, www.rcsb.org (PDB ID code 1GKA).

‡Present address: Institute of General and Ecological Chemistry, Technical University of Łodz, Zwirki 36, 90-924 Łodz, Poland.

‖To whom reprint requests should be addressed. E-mail: john.helliwell@man.ac.uk.

BIOPHYSICS

and insecticyanin (13) fold the larger biliverdin ligand to fit within the calyx. In contrast, the crystal structure of β-CR presented here reveals the binding sites of the two carotenoids to span the interface between two monomers, and thereby the three-dimensional structural basis of the spectral shift depends on heterodimer formation.

Materials and Methods

Purification and Crystallization. α-CR was extracted from finely ground lobster carapace and purified by ion exchange chromatography (14). The protein was dissociated into β-CRs by extensive dialysis against 0.3 mM Tris·HCl, pH 8.8. The relevant β-CR [$\beta(A_1/A_3)$] was resolved from the mixture of dimers by fast protein liquid chromatography. This involved a MonoQ HR10/10 column with linear gradients (0–25% B in 3 ml followed by 25–100% B in 100 ml) made from buffer A (10 mM Tris·HCl, pH 7) and buffer B (10 mM Tris·HCl/0.2 M KCl, pH 7) and run at 1.0 ml·min^{-1}. Crystals were grown in microbatch under oil (15). Extensive crystallization experiments using the vapor diffusion technique failed. The best crystals were grown at 4°C in 2- to 4-μl drops under oil containing final protein concentrations of 10 mg/ml in 10 mM Tris·HCl buffer (pH 8.0) and 1.25 M (NaH_2/K_2H) PO_4 at pH 7 in 0.05 M Hepes buffer at pH 7.5. The solutions remained clear for several weeks. Crystals required 4 months to reach a size of 0.45 × 0.12 × 0.1 mm and were vivid blue, almost black (dark blue is the expected color for absorption around 570–580 nm). The absorption maximum of the β-CR remains at 580 nm at room temperature in this crystallization buffer.

X-Ray Data Collection, Structure Solution, and Refinement. Crystallographic x-ray data were collected at 100°K at the Daresbury SRS 2.4 T *M*ulti-*P*ole *W*iggler beamline (MPW) 14.1 (16), by using an Area Detector Systems (San Diego) 2 × 2 Q4 charge-coupled device area detector set 168 mm from the crystal with zero tilt angle. The exposure time was 90 sec per 1° frames at a wavelength of 1.488 Å. A total of 60 high-quality diffraction images were recorded. Data processing was done with DENZO/SCALEPACK (17); the space group was determined as $P6_322$ with refined unit cell dimensions of a = b = 155.5 Å and c = 168.5 Å. A total of 24,504 unique observations (99.7% complete) to 3.0 Å were derived from 171,943 observations with an average merging R of 12.4% (35.0% in the range 3.38–3.23 Å, with completeness 100.0%), and average $I/\mathrm{sig}(I)$ of 15.5 (5.5 between 3.38 and 3.23 Å). The completeness was near 100% across all resolution ranges. The statistics for the last two-resolution shells reduced their usefulness [percent of reflections with $I>3\sigma(I)$ = 41% and R_{merge} of 55.5% in the 3.23- to 3.11-Å shell, and respectively 27% and 81% for these two parameters in the 3.11- to 3.0-Å shell]. The clarity of the electron density maps to 3.23 and 3.0 Å was also checked and found to be only marginally different. Thereafter, the resolution limit was set to 3.23 Å for the structure solution and refinement, comprising 19,698 unique reflections.

The unit-cell dimensions indicate a molecular volume of 7.55 Å^3/Da if only one 40-kDa A_1/A_3 dimer is contained in an asymmetric unit, well outside the usual range of this value. The fraction of unit-cell volume occupied by protein atoms would be 16.4%. The large solvent content, in excess of 83%, would explain the weak diffraction to 3.2 Å. Indeed, structure solution using the molecular replacement program AMORE (18), as implemented in the CCP4 package (19), verified the occurrence of only one dimer per asymmetric unit. The 1.4 Å refined model of apoCR A_1 (20) was used as search model in the polyalanine form. There were two clear solutions from which the unit cell packing was determined. The solutions were subjected to rigid body refinement by using REFMAC (21). The side chains of the A_1 amino acid sequence were added to one, and the A_3 subunit sequence was modeled by homology onto the Cαs of the other solution. Refinement was continued by using CNS (22). Maps were inspected with the graphics packages O (23) and OOPS2 (24). AXT coordinates, in the 6-s-cis form, were downloaded from the National Cancer Institute Drug Information System three-dimensional database (25) and built into the $2F_o - F_c$ electron density map, in the appropriate places.

Table 1. X-ray structure refinement details

Crystallographic R_{factor} (R_{free})*	21.3 (25.1)
No. of protein atoms (a.u.)	2,847
No. of nonprotein atoms (a.u.)	149
Average temperature factors for protein atoms, (B) Å^2	41.9
rms deviation from target values:	
Bonds, Å	0.031
Angles, °	2.78
Dihedrals, °	26.6
Improper, °	1.53

a.u., asymmetric unit.

*Free R_{factor} was calculated by using a 5% subset of the data, chosen at random and excluded from refinement.

The AXT conformations (6-*s-trans*) were determined via examination of atomic B factor values for the four end-ring atoms: in the 6-*s-trans* conformation, B factors were lower by 25% than those in the 6-s-cis conformation. The hand of the hydroxy substituents at each end ring was determined by using omit maps. Between the two AXTs there was a patch of difference electron density; attempts to fit a Hepes molecule there failed, but dodecane (i.e., from the paraffin oil) fitted better, although with high B factors (>80 Å^2). A gas chromatography analysis revealed a mixture of C22, C24, and C26 for this oil. Further evidence that it is a hydrocarbon is that it sits between two surface-exposed Phe residues [Phe-101 (A_1) and Phe-99 (A_3)], which are also unusual and suggest a site of oligomerization toward α-CR via hydrophobic-to-hydrophobic interactions (as proposed later). The bound waters were located in the ($F_o - F_c$) difference Fourier map contoured at 4σ and where sensible hydrogen bond partners existed. A total of 30 waters were found with final B factors ranging from 24 to 62 Å^2. The end-ring cavity waters W1 and W2 had B factors of 38 and 52, respectively, and peak at 6σ in ($F_o - F_c$) maps but did not appear in ($2F_o - F_c$) maps at the 1 rms level. We thus describe these waters as relatively loosely bound compared with other bound waters (approximately 70% of the bound waters appeared in both $2F_o - F_c$ *and* $F_o - F_c$ maps). The H bond distances of W1 and W2 are short signifying their importance in the binding to the 4- and 4′-keto oxygens of each AXT, and are shown in Fig. 4 *c* and *d*. W1 is also observed in the 1.4 Å resolution A_1 apoCR (both subunits) in the same position within 0.5 Å. The final β-CR model has R_{factor} 21.3% and R_{free} 25.1% and consists of 354 aa residues, 30 ordered waters, one Hepes molecule, one dodecane molecule, and one Tris·HCl. Hepes, dodecane, Tris·HCl coordinates were downloaded from the HIC-UP database (26). Refinement statistics are given in Table 1. The Ramachandran plot of the heterodimer (not shown) has 255 nonglycine residues in the most favored regions (80.3%), 60 residues in the additional allowed region (19.0%), 1 residue [Tyr-112 (A_1)] in the generously allowed region (0.3%), and 1 residue [Tyr-110 (A_3)] in the disallowed region (0.3%). This confirms that it is a feature of the lipocalin family to have these two residues as outliers (20). The secondary structure elements were assigned by PROCHECK (27). For monomer A_1, these are an α-helix (16–24), β strand A1 (residues 33–36), A2 (37–41), B (50–58), C (63–70), D (76–85), E (93–95), F1 (103–106), F2 (107–110), G (115–123), H (128–137), an α-helix (147–154) and a β strand I (164–166). For monomer A_3 there are β strands labeled A1 (residues 28–31), A2

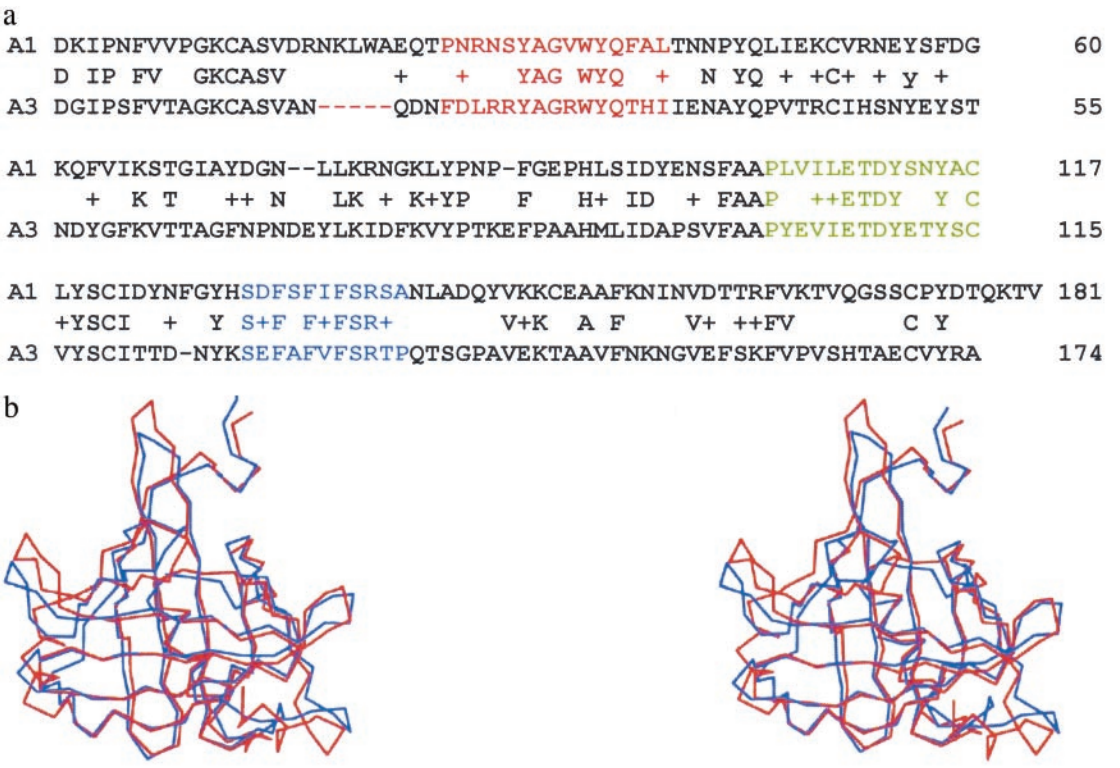

Fig. 2. (*a*) Alignment of the A_1 and A_3 amino acid sequences. The lipocalin consensus regions of the amino acid sequences are color coded [residues 25–40 (A_1), 20–35 (A_3), red; 103–117 (A_1), 101–115 (A_3), green; 129–140 (A_1), 126–137 (A_3), blue]. (*b*) Overlay of the A_1 and A_3 Cαs in stereo showing the common lipocalin fold and the differences in the loop regions.

(32–35), B (45–54), C (59–67), D (73–81), E (90–94), F1 (101–104), F2 (105–108), G (113–121), H (125–134), and an α-helix (142–154). The rms deviations of the AXTs from their starting conformation are 2.1 Å for AXT1 and 2.2 Å for AXT2. The rms deviation between the A_1 unbound protein structure (20) and the A_1 AXT bound form here is 2.2 Å (all atoms) or 1.6 Å (Cαs). If the flexible N terminus (14 residues) is excluded, the rms on Cαs is 0.63 Å. Some further large shifts in position at the A_1-binding site were also observed (see *Results and Discussion*). The unbound form of the A_3 subunit is not known, so the effect of binding on atomic positions cannot be estimated. Figures were prepared using MOLSCRIPT (28).

Results and Discussion

β-CR Structure. The crystal structure of β-CR involves a heterodimer of A_1 and A_3 protomers in the crystal asymmetric unit. The A_1 protein has 180 residues, and the A_3 protein has 174 residues; the two molecules have 35% sequence identity (Fig. 2*a*). Both subunits have the typical topology of a lipocalin (Fig. 2*b*) with a β barrel made up of two distinct β sheets (29). β sheet I consists of β strands A1, B, C, D, E, and F1. β sheet II consists of β strands A2, F2, G, and H. The average rms deviation between common Cαs of the two monomers is 1.1 Å. The A_1 and A_3 subunits interact via a loop region, connecting strands G and H of each subunit (Fig. 3*a*). This dimerization is different from that of the A_1/A_1 crystal structure, which is achieved via a close contact between the two strands F of each subunit (20).

The Bound Carotenoids. The two bound carotenoids interpenetrate the A_1 to A_3 interface, with each subunit containing half of each carotenoid (Fig. 3*a*). The AXTs are labeled AXT1, where ring C1–6 is within the calyx of A_1, and AXT2 with ring C1–6 within the calyx of A_3. The carotenoids approach within 7 Å at the central portions of their polyene chains. The two refined bound AXTs have very similar all-trans conformations (rms deviation 0.3 Å), with a marked bow shape. Fig. 3 *b* and *c* shows the plan and edge views of AXT1 starting and refined models superimposed on ($F_o - F_c$) difference density. The end rings are now essentially coplanar with their polyene chains, whereas the conformation of canthaxanthin, the closest relative for which there is a known crystal structure in an unbound form, has dihedral angles of around −43° (30). It is possible to discern the bowing and end-ring coplanarization in this map because of the high-quality, 100% completeness and multiplicity of the data. The density around AXT2 (not shown) is of equally high quality. Fig. 3*d* shows the calculated AXT potential energy as a function of the torsion angle between the end ring and the polyene chain (31).

The protein environment of each carotenoid (Fig. 4 *a* and *b*) is asymmetric with the two end rings of each AXT having dissimilar environments. For AXT1 the environment for its C1–6 ring (Fig. 4*c*) has as neighbors hydrophilic residues Gln-46 (A_1) and Asn-54 (A_1), which hydrogen bond to the hydroxyl group O3. Tyr-56 (A_1) and Tyr-97 (A_1) tether a bound water molecule (W1 in our Protein Data Bank file, IGKA), very close to AXT1 O4 at 2.60 Å that, together with Asn-54 (A_1), are responsible for the coordination of the ring keto-oxygen O4. Other hydrophilic residues are Gln-37 (A_1) and Ser-67 (A_1). In this end-ring cavity, several hydrophobic residues are also present, namely Val-52 (A_1), Ile-65 (A_1), Ile-95 (A_1), Phe-134 (A_1), and Phe-136 (A_1). All these residues and W1 show little movement on binding of AXT1 (between 0.3 and 1.0 Å) compared with the residues around the C1′-6′ ring (see below). The AXT2 C1–6 ring pocket (Fig. 4*d*) is defined by Gln-41 (A_3) and Thr-64 (A_3), which coordinate the hydroxylic oxygen O3 and the carbonyl oxygen O4, respectively. As with AXT1, a bound water molecule (W2 in our Protein Data Bank file, IGKA) is found, very close (2.73 Å) to the AXT2 keto-oxygen O4, and is tethered

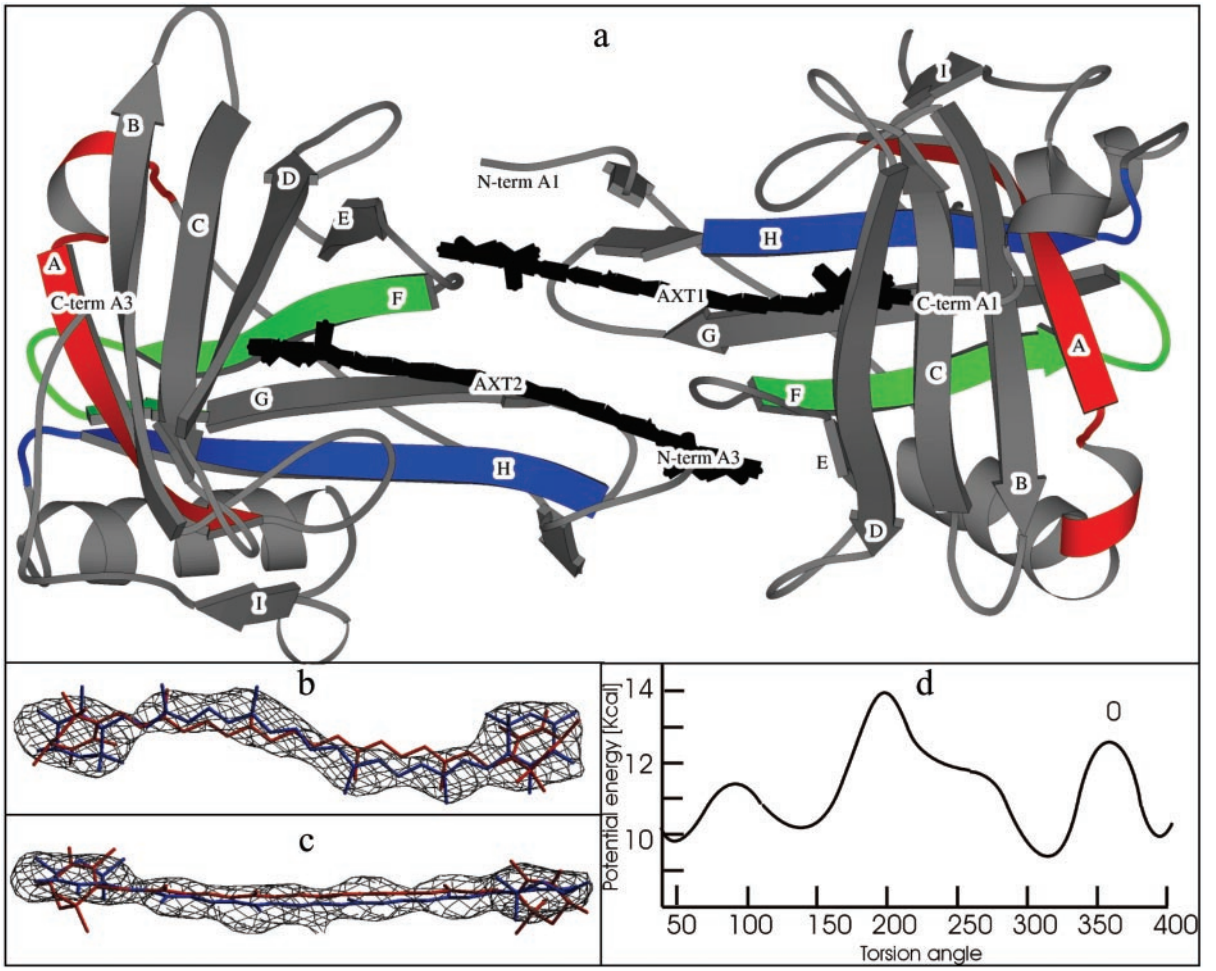

Fig. 3. (*a*) The structure of the A_1/A_3 dimer assembly (in ribbon format) with the two bound carotenoids (in ''stick'' format, colored black). The individual β strands are color coded according to the consensus regions. (*b*) Superposition of AXT1 starting (red) and refined (blue) models on ($F_o - F_c$) difference density. (*c*) Edge view of *b*. (*d*) Graphical representation of the calculated potential energy in AXT as a function of the torsion angle between the end ring and the polyene chain. [Reproduced with permission from ref. 31 (Copyright 1994, Birkhäuser Basel)].

by hydrogen bonds to Ser-49 (A_3) and Tyr-51 (A_3). Gln-32 (A_3) participates in the overall hydrogen bonding. The presence of Ile-76 (A_3), Phe-78 (A_3), Phe-131 (A_3), Phe-133 (A_3), and Val-62 (A_3) makes the remainder of the cavity hydrophobic.

The AXT1 ring C1′-6′ (Fig. 4*e*) is in a small cavity of the A_3 protein. The keto-oxygen O4′ and the hydroxyl oxygen O3′ are close to NE2 of His-90 (A_3), which is the only hydrophilic residue in a pocket that also contains Phe-86 (A_3), Phe-126 (A_1), Ile-3 (A_1), and Tyr-128 (A_1). Comparison with the previously determined A_1 unbound form (20) shows that the residues involved in binding undergo substantial movement (between 3.7 and 9.5 Å). The AXT2 ring C1′-6′ environment (Fig. 4*f*) is similar to that of AXT1, where its keto-oxygen O4′ and the hydroxyl oxygen O3′ are close to NE2 of His-92 of subunit A_1. The hydroxyl oxygen O4′ is also coordinated to the Ser-94 (A_1) OH and close to Asn-86 (A_1) OD1. Other residues present are Thr-122 (A_3), Asp-123 (A_3), Glu-90 (A_1), Ile-3 (A_3), and Tyr-125 (A_3). This binding site is more accessible to water molecules than the corresponding one for AXT1, where residues Phe-126 (A_1) and Phe-86 (A_3) close a water-accessible channel (Fig. 4 *a* vs. *b*).

The AXT polyene chains, C7 to C7′ (Fig. 1), are held in a sterically favorable manner relative to many hydrophobic residues. So for AXT1, Pro-4(A_1), Phe-6(A_1), Val-7(A_1) Tyr-45(A_1), Tyr-124(A_1), and Phe-132(A_1) make a central cavity for binding, including locking the central methyl groups C20 and C20′ (Fig. 4*a*). For AXT2, there is an equivalent set of hydrophobic residues, namely, Pro-4(A_3), Phe-6(A_3), Tyr-40(A_3), Ile-93(A_3), and Phe-129(A_3) (Fig. 4*b*). Phe-101 (A_1), Pro-104 (A_1), Ile-122 (A_1), Phe-99 (A_3), Pro-102 (A_3), and Ile-120 (A_3) are sandwiched between the two carotenoids (Fig. 4 *a* and *b*). Some of the A_1 residues move substantially on binding (Phe-6 by 3.6 Å; Pro-4 by 6.7 Å; Val-7 by 3.6 Å; Phe-101 by 6.2 Å). A similar comparison cannot be made for A_3, because its unbound structure has not been determined. The polyene chains are close to each other, and this would facilitate the exciton interaction, evident from CD spectroscopy (2, 4). Resonance Raman spectroscopy shows that this does not, however, contribute to the spectral shift (3, 4), which would require yet closer interaction. The whole arrangement cannot take place without the central C20 and C20′ methyls firmly interacting with the protein, as is revealed by the structure, thereby centering the AXTs in position.

The two AXT-binding sites have many conserved amino acid residues, as well as the two bound waters W1 and W2, serving similar functions. Fig. 4 *c* and *d* show interactions between the end ring (C1–6) and the protein (residues in brackets are from subunit A_3): Gln-46 (Gln-41), Phe-134 (Phe-131), Phe-136 (Phe-133), Gln-37 (Gln-32), Tyr-56 (Tyr-51), and Ile-95 (Ile-93). In addition, there are conservative amino acid mutations from A_1 to A_3 (latter in brackets) for Leu-40 (Ile-35), Val-52 (Ile-47), and Ser-67 (Thr-64), whereas Asn-54 is mutated to Ser-49 and Tyr-97

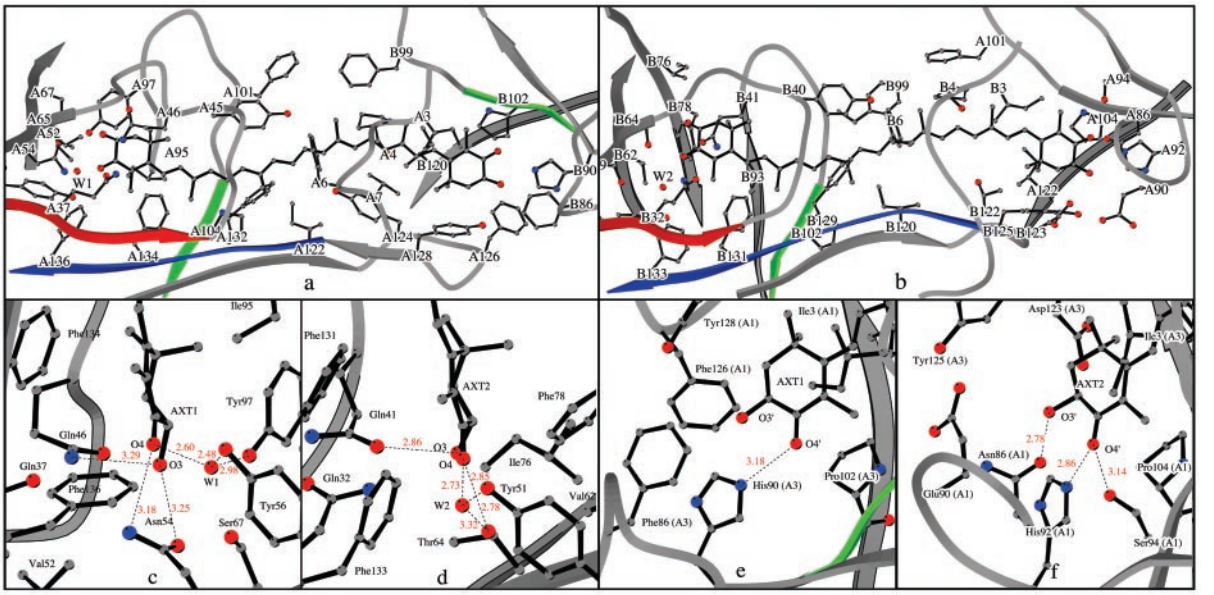

Fig. 4. Schematic of the structural details with key distances in Å between atoms indicated in red. A denotes residues from A_1, B residues from A_3. (*a*) The complete binding site for carotenoid AXT1. (*b*) The complete binding site for carotenoid AXT2. (*c*) Details of ring C1–6 AXT1 binding site. (*d*) Details of ring C1–6 AXT2 binding site. (*e*) Details of ring C1′-6′ AXT1 binding site. (*f*) Details of ring C1′-6′ AXT2 binding site.

is substituted by Phe-78 in A_3. Considering the environment of the rings C1′-6′ (Fig. 4 *e* and *f*) the only conserved residues between A_1 and A_3 (latter in brackets) are His-92 (His-90), Pro-104 (Pro-102), and Tyr-128 (Tyr-125). The hydrophilic C1′-6′ ring-binding site for AXT2 becomes hydrophobic for AXT1 with the mutation of Thr-94 (A_1) to Leu-92 (A_3), Glu-90 (A_1) to Phe-86 (A_3). Most significantly, there is a water molecule in close contact with one of the two keto-oxygens of each AXT. Indeed, both waters are in equivalent positions by the A_1/A_3 protein dimer noncrystallographic 2-fold symmetry. Moreover, in the A_1 subunit, W1 is within 0.5 Å of a water molecule observed in the apoCR A_1 structure, determined at the much higher resolution of 1.4 Å. The W1 position was occupied in both crystallographically independent A_1 monomers of that form (20). Such a water site is not present in the predicted β-CR structure (7).

The Structural Basis of the Bathochromic Shift. The bathochromic shift appears, then, to be the result of several different perturbations of the carotenoid. First, the end rings are now essentially coplanar with the polyene chain (Fig. 3*c*), thus extending the conjugation, even though energetically less favorable (31) and altering the electronic ground state. This is similar to the case of sensory rhodopsin II where the β-ionone ring is also made coplanar with the polyene chain (32). Second, the end-ring keto-oxygens are within hydrogen bonding distance of two bound waters and two His nitrogens (Fig. 4). The resultant polarization of the ligand may thus result in AXT acquiring a permanent induced dipole moment (3). These waters are not the most ordered that are observed and would be relatively easy to remove on dehydration, and may thus relax the end rings to become noncoplanar with the polyene chains. This effect can also be produced by the loss of tertiary protein structure on denaturation. The increased conjugation on ring coplanarization would partly explain the bathochromic shift (33). However, additional electronic delocalization of the polyene conjugation because of the W1, W2, His-92 (A_1), and His 90 (A_3) hydrogen bonds to the keto-oxygens is needed. The proposition (4) that a bound water molecule would be involved in this aspect is supported, therefore, and its exact position reported. The asymmetric environment at each end of the carotenoids explains the finding that the reduction of the keto-oxygens proceeds at different rates (2), as predicted from spectroscopy (5). The two docking sites for the carotenoids force the marked bowing of each carotenoid. Quantum calculations can explore whether, and how much, the bowing of the carotenoids contributes to the bathochromic shift. Final tuning of the spectral bathochromic shift of the β-CR could come from the protein environment itself, because we know, for example, that the AXT absorption peak in hexane vs. pyridine is different by 20 nm, thought to be a function of refractive index (2). The close proximity of the π-orbitals of the nearby aromatic side chains could provide this. The paucity of charged residues in the immediate vicinity of the carotenoids probably rules out electrostatic interaction as a contributor to the spectral shift and contrasts with the situation in rhodopsin. But, overall, the bathochromic shift effect to 580 nm is explained by the β-CR structure.

A final shift to 630 nm is provided by α-CR, which is thought to consist of either a dimer of tetramers of β-CRs or a spiral (34). The β-CR crystal has an open packing of A_3 trimers in the *xy* plane, perpendicular to layers of A_1 dimers along the *z* axis. Most of the interactions involve A_3 trimers around the crystallographic 3-fold: residues Asn-20 with Thr-167 and Cys-170′; Asp-22 with Tyr-31′, Arg-29′ and Tyr-172′; Arg-24 with Asn-50′. The strongest interactions of the A_1 dimers, around the crystallographic 2-fold involve Asn-75 with Asn-75′ and Thr-177 with Thr-180′. Lattice contacts are made by Lys-61 (A_1) with Glu-157 (A_3) and Ser-159 (A_3). This pair is linked to similar pairs through crystallographic symmetry, but this packing is "infinitely" long and, therefore, cannot resemble live α-CR. A structural mechanism is required to terminate a cluster, after eight β-heterodimers have been assembled to form the α-CR. Interestingly, the β-heterodimer structure has a surface-exposed hydrophobic patch (A_1 Phe-6, A_1 Phe-101, and A_3 Phe-99), in the center of the molecule near the AXT-binding sites (Fig. 4 *a* and *b*), which is a possible candidate for further subunit–subunit interaction. Although a plausible oligomerization mechanism is via association of heterodimers at this place of contact, additional factors must be involved because β-CR is an irreversibly formed dissociation product from α-CR.

Concluding Remarks. In summary, the structural basis for the bathochromic shift of the carotenoid spectrum in lobster β-CR has been revealed by this study. It is now apparent how lobster is structurally able to utilize AXT to produce blue/purple pigments for camouflage. The structural nature of the protein component enabling this effect may well be different in different animals or phyla, but structural studies on this diverse group of invertebrate carotenoproteins are sparse. Molecular designers can now take advantage of our results in the synthesis of new molecules such as carotenoids encapsulated in rigid-rod β barrels (35), e.g., for use as food colorants or dyestuffs with a designed bathochromic shift. The primary parameters to be varied in such designs would involve end-ring coplanarization with the polyene chains and hydrogen bonding to the keto-oxygens. Moreover, a means of targeted delivery of AXT, normally very insoluble in aqueous systems, as a drug for various diseases (www.astaxanthin.org) is now possible. Also, insight has been gained, at the molecular level, into the effect of cooking (and dehydration), where denaturation of the β-CR can lead to relaxation of the clasp of the AXT. Dehydration is reversible, although the coloration change is similar to that after cooking. The latter must involve complete and irreversible denaturation.

We are very grateful to George Britton (University of Liverpool), John Sutherland, and Jonathan Clayden (University of Manchester) for helpful discussions. We thank SRS Daresbury Laboratory and the Joint Biology Program of the U.K. Research Councils for synchrotron radiation beamtime. We are grateful for the award of a research grant from the Leverhulme Trust. We thank the Engineering and Physical Sciences Research Council and the University of Manchester for a Ph.D. studentship for M.C. The Wellcome Trust and the Biotechnology and Biological Sciences Research Council funded the Manchester Structural Chemistry Laboratory computing and graphics suite.

1. Wald, G., Nathanson, N., Jencks, W. P. & Tarr, E. (1948) *Biol. Bull. (Woods Hole, MA)* **95,** 249–250.
2. Buchwald, M. & Jencks, W. P. (1968) *Biochemistry* **7,** 844–859.
3. Salares, V. R., Young, N. M., Bernstein, H. J. & Carey, P. R. (1979) *Biochim. Biophys. Acta* **576,** 176–191.
4. Britton, G., Weesie, R. J., Askin, D., Warburton, J. D., Gallardo-Guerrero, L., Jansen, F. J., de Groot, H. J. M., Lugtenburg, J., Cornard, J.-P. & Merlin, J.-C. (1997) *Pure Appl. Chem.* **69,** 2075–2084.
5. Weesie, R. J., Verel, R., Jansen, F. J. H. M., Britton, G., Lugtenburg, J. & de Groot, H. J. M. (1997) *Pure Appl. Chem.* **69,** 2085–2090.
6. Krawczyk, S. & Britton, G. (2001) *Biochim. Biophys. Acta* **1544,** 301–310.
7. Keen, J. N., Caceres, I., Eliopoulos, E. E., Zagalsky, P. F. & Findlay, J. B. C. (1991) *Eur. J. Biochem.* **202,** 31–40.
8. Quarmby, R., Norden, D. A., Zagalsky, P. F., Ceccaldi, H. J. & Daumas, R. (1977) *Comp. Biochem. Physiol.* **56B,** 55–61.
9. Bourne, H. R. & Meng, E. C. (2000) *Science* **289,** 733–745.
10. Palczewski, K., Kumasaka, T., Hori, T., Behnke, C. A., Motoshima, H., Fox, B. A., Le Trong, I., Teller, D. C., Okada, T., Stenkamp, R. E., *et al.* (2000) *Science* **289,** 739–745.
11. Newcomer, M. E. & Ong, E. O. (2000) *Biochim. Biophys. Acta* **1482,** 57–64.
12. Huber, R., Schneider, M., Epp, O., Mayr, I., Messerschmidt, A., Pflugrath, J. & Kayser, H. (1987) *J. Mol. Biol.* **195,** 423–434.
13. Holden, H. M., Rypniewski, W. R., Law, J. H. & Rayment, I. (1987) *EMBO J.* **6,** 1565–1570.
14. Chayen, N. E., Gordon, E. J., Phillips, S. E. V., Saridakis, E. E. G. & Zagalsky, P. F. (1996) *Acta Crystallogr. D* **52,** 409–410.
15. Chayen, N. E., Stewart, P. D. S., Maeder, D. L. & Blow, D. M. (1990) *J. Appl. Crystallogr.* **23,** 297–302.
16. Duke, E. M. H., Kehoe, R. C., Rizkallah, P. J., Clarke, J. A. & Nave, C. (1998) *J. Synchrotron Rad.* **5,** 497–499.
17. Otwinowski, Z. & Minor W. (1997) *Methods Enzymol.* **276,** 307–326.
18. Navaza, J. (1994) *Acta Crystallogr. A* **50,** 157–163.
19. Collaborative Computational Project No. 4 (1994) *Acta Crystallogr. D* **50,** 760–763.
20. Cianci, M., Rizkallah, P. J., Olczak, A., Raftery, J., Chayen, N. E., Zagalsky, P. F. & Helliwell, J. R. (2001) *Acta Crystallogr. D* **57,** 1219–1229.
21. Murshudov, G. N., Vagin, A. A. & Dodson, E. J. (1997) *Acta Crystallogr. D* **3,** 240–255.
22. Brünger, A. T., Adams, P. D., Clore, G. M., DeLano, W. L., Gros, P., Grosse-Kunstleve, R. W., Jiang, J.-S., Kuszewski, J., Nilges, M., Pannu, N. S., *et al.* (1998) *Acta Crystallogr. D* **54,** 905–921.
23. Jones, T. A., Zou, J. Y., Cowan, S. W. & Kjeldgaard, M. (1991) *Acta Crystallogr. A* **47,** 110–119.
24. Kleywegt, G. J. & Jones, T. A. (1996) *Acta Crystallogr. D* **52,** 829–832.
25. Milna, G. W. A., Nicklans, M. C., Driscoll, J. S., Wang, S. & Zaharevitz, D. (1994) *J. Chem. Inf. Comput. Sci.* **34,** 1219–1224.
26. Kleywegt, G. J. & Jones, T. A. (1998) *Acta Crystallogr. D* **54,** 1119–1131.
27. Laskowski, R. A., McArthur, M. W., Moss, D. S. & Thornton, J. M. (1993) *J. Appl. Crystallogr.* **26,** 283–291.
28. Kraulis, P. J. (1991) *J. Appl. Crystallogr.* **24,** 946–950.
29. Flower, D. R., North, A. C. T. & Sanson, C. E. (2000) *Biochim. Biophys. Acta* **1482,** 9–24.
30. Bart, J. C. J. & MacGillavry, C. H. (1968) *Acta Crystallogr. B* **24,** 1587–1606.
31. Britton, G., Pfander, H. & Birkhauser, S. L. J., eds. (1994) in *Carotenoids* (Birkhäuser, Basel), Vol. 1B, pp. 69–73.
32. Luecke, H., Schobert, B., Lanyi, J. K., Spudich, E. N. & Spudich, J. L. (2001) *Science* **293,** 1499–1503.
33. Clayden, J., Greeves, N., Warren, S. & Wothers, P. (2001) *Organic Chemistry* (Oxford Univ. Press, Oxford).
34. Zagalsky, P. F. & Jones, R. (1982) *Comp. Physiol. Biochem.* **71b,** 237–242.
35. Baumeister, B. & Matile, S. (2000) *Chem. Eur. J.* **6,** 1739–1749.